JOURNAL OF PROPULSION AND POWER
Vol. 21, No. 3, May–June 2005

Ablative Z-Pinch Pulsed Plasma Thruster

Thomas E. Markusic,* Kurt A. Polzin,† and Edgar Y. Choueiri‡
Princeton University, Princeton, New Jersey 08544
and
Michael Keidar,§ Iain D. Boyd,¶ and Neal Lepsetz**
University of Michigan, Ann Arbor, Michigan 48109

The design, performance, and basic features of ablative pulsed plasma thrusters based on the z-pinch configuration are discussed through a series of experiments and numerical simulations. The motivation stems from the promise of the z-pinch configuration for increasing the thrust-to-power ratio and mass utilization efficiency above those of ablative thrusters with a conventional rectangular geometry. The performance of a series of ablative z-pinch pulsed plasma thrusters is characterized using a swinging-gate thrust stand and mass ablation measurements. The performance measurements are complemented by additional experimental diagnostics (current monitoring and high-speed photography) and numerical modeling in order to gain an understanding of the acceleration mechanism and provide direction for future design iterations. Three iterations in the design of the thruster result in thrust-to-power ratios ranging from 12–45 μN/W, with specific impulse and thrust efficiency values spanning 240–760 s and 2–9%, respectively. Numerical simulations show reasonable quantitative agreement with the experimental data and predict the existence of an optimal thrust chamber aspect ratio, which maximizes the thrust-to-power ratio.

Nomenclature

A	=	cross-sectional area, m^2
C	=	thruster capacitance, F
I_{bit}	=	impulse bit, N-s/shot
I_{sp}	=	specific impulse, s
j_a	=	anode tip current density, A m^{-2}
j_{av}	=	average current density, A m^{-2}
k	=	Boltzmann's constant, J K^{-1}
L_0	=	initial thruster inductance, H
l	=	Polytetrafluoroethylene chamber length, m
m	=	mass, kg
m_{bit}	=	mass bit, kg/shot
n_e	=	electron number density, m^{-3}
n_1, n_2	=	density, m^{-3}
P	=	pressure, N m^{-2}
Q_F	=	particle flux heating, K m^{-3} s^{-1}
Q_J	=	Joule heating, K m^{-3} s^{-1}
Q_r	=	radiation heating, K m^{-3} s^{-1}
R_1, R_2	=	chamber inner/outer radius, m
T_e	=	electron temperature, K
T_1, T_2	=	temperature, K
T/P	=	thrust to power, N W^{-1}
t, τ	=	time, s
V_1, V_2	=	velocity, m s^{-1}
z	=	axial distance, m
α	=	j_{av}/j_a
Γ	=	ablation rate, kg m^{-2} s^{-1}
Δ	=	length, m
Δv	=	characteristic mission velocity, m s^{-1}
η_t	=	thrust efficiency, %
μ	=	permeability, H m^{-1}
ρ	=	initial plasma density, m^{-3}

Received 5 August 2003; revision received 10 April 2004; accepted for publication 10 May 2004.

*Graduate Research Assistant, U.S. Air Force Palace Knight, Electric Propulsion and Plasma Dynamics Laboratory (EPPDyL), Mechanical and Aerospace Engineering Department, Engineering Quadrangle, Olden St.; currently Research Scientist, NASA Marshall Space Flight Center, Huntsville, Alabama 35812. Member AIAA.

†Graduate Research Assistant, National Defense Science and Engineering Graduate Fellow, Electric Propulsion and Plasma Dynamics Laboratory (EPPDyL), Mechanical and Aerospace Engineering Department, Engineering Quadrangle, Olden St. Member AIAA.

‡Chief Scientist at EPPDyL and Associate Professor, Applied Physics Group, Electric Propulsion and Plasma Dynamics Laboratory (EPPDyL), Mechanical and Aerospace Engineering Department, Engineering Quadrangle, Olden St.; choueiri@princeton.edu. Associate Fellow AIAA.

§Research Scientist, Department of Aerospace Engineering, François-Xavier Bagnoud Building, 1320 Beal Ave. Member AIAA.

¶Associate Professor, Department of Aerospace Engineering, François-Xavier Bagnoud Building, 1320 Beal Ave. Senior Member AIAA.

**Undergraduate Student, Department of Aerospace Engineering, François-Xavier Bagnoud Building, 1320 Beal Ave.

I. Introduction

THERE is presently a renewed interest in pulsed plasma thrusters (PPTs), especially ablative PPTs, for a wide range of space missions (for example, see Burton and Turchi[1] and Martinez-Sanchez and Pollard[2]). These thrusters have been considered for constellation maintenance of sparse-aperture interferometers[3] and were recently flown on a mission demonstrating formation flying.[4] The benefits of PPTs are their small impulse bits ($\sim 10^{-4}$ N-s), which allow for precise control of satellite motion, reliability, and low overall power usage. Two classifications of PPTs exist, corresponding to the form of propellant used: gas-fed (GFPPT) or ablative (APPT). The gas-fed variant has the advantages of a "clean" exhaust plume because it is able to use inert gases as propellants and high specific impulse. The ablative version uses a solid propellant, such as Teflon®, to provide advantages such as compactness and overall ease of system integration. APPTs also provide larger impulse bits than their gas-fed counterparts. However, contamination of the spacecraft by the plume and the lower specific impulse might limit the missions for which APPTs are suitable.

Compared to gas-fed PPTs, ablative PPTs are better suited for providing high-thrust, low-Δv maneuvers on spacecraft that are power limited. An APPT, which requires no tankage or propellant feed lines, can operate at a lower specific impulse and a higher thrust-to-power ratio (T/P) than a GFPPT, yet still possess a lower total system mass (for a given Δv). This advantage disappears for larger Δv missions, which require more propellant. Although there exist many missions, such as attitude correction and high slew-rate maneuvers, where the APPT has an advantage over the gas-fed variant, additional work is needed to improve their thrust to power at

low power. The main motivation for developing the ablative Z-pinch PPT (AZPPT) was to create a thruster for such missions, with higher thrust-to-power ratios than more common PPT designs, by exploiting certain favorable attributes of the z-pinch geometry.

High T/P can be attained not only by increasing thrust, but also by decreasing the power consumption, that is, by increasing the thrust efficiency at a given I_{sp}. There are two broad categories of inefficiencies in ablative pulsed plasma thrusters that limit thrust efficiency. These include energy inefficiencies, which pertain to the efficient transfer of stored capacitor energy into acceleration of the ionized propellant, and propellant utilization inefficiencies, which include particulate emission and late-time vaporization.[5] We employed the z-pinch geometry in an attempt to increase the overall thrust efficiency by ameliorating the problem of particulate emission.

In the following section the details of the AZPPT design are presented. Next, the apparatus used to carry out experimental measurements is described, and then, the experimental results are presented. A numerical model that aimed to descibe the AZPPT acceleration mechanism and to predict performance follows. Finally, the results are summarized, and future plans are outlined.

II. Ablative Z-Pinch PPT

A. Description

Z pinches were originally conceived of as a method for producing hot, dense plasmas for nuclear fusion research.[6] In the 1960s, Jahn et al.[7] showed that the z-pinch geometry could be modified to create an axially streaming plasma, thus yielding a new type of plasma thruster. This was accomplished by replacing one of the electrodes in the conventional z-pinch geometry with an electrode that had an orifice at its center. It was shown that, after the radial pinching phase, plasma was ejected axially with speeds comparable to the initial pinching speed.

The AZPPT is structurally very similar to its gas-fed counterpart. The difference is that the sidewalls, aside from providing electrical insulation, also serve as the source of propellant. However, the acceleration mechanism in the AZPPT is not yet fully understood and might, in fact, be quite different from that observed in the gas-fed devices.

The geometry and components of the AZPPT are schematically illustrated in Fig. 1. The discharge chamber consists of a solid inner electrode (anode) and a hollow outer electrode (cathode) with an orifice. The space between the electrodes is occupied by a hollow cylindrical bar of polytetrafluoroethylene (PTFE) propellant. Operation of the thruster is achieved by charging the capacitor to a desired voltage and then firing the igniters (usually arrayed in equally spaced azimuthal locations as illustrated in Fig. 1). In the absence of a gaseous propellant, the igniters provide enough charge carriers to initiate a breakdown, which allows current to start flowing from the capacitor. A cylindrical current sheet rapidly forms at the surface of the propellant wall, ablates the PTFE, and accelerates its products radially inward. The current sheet dynamics for ablative thrusters are not well understood, and so it is unclear whether the current sheet collapses radially inward as in the gas-fed thruster (detonation mode) or if it remains relatively stationary, heating and electromagnetically "blowing" propellant radially inward (deflagration mode). Furthermore, without understanding the current sheet dynamics, it is uncertain how the propellant flow is "turned" to obtain axial ejection from the cathode orifice. Ultimately, though, exhaust gas is ejected from the cathode orifice, and thrust is derived. Discharging the thruster over many pulses causes the propellant to recede until it reaches the outer wall, at which point the propellant supply is exhausted.

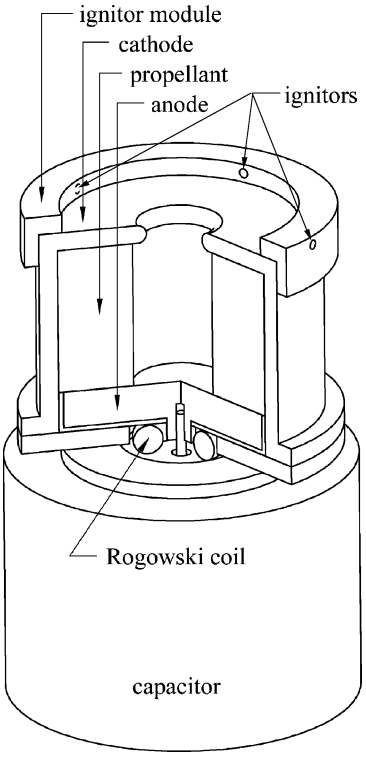

Fig. 1 Schematic of the AZPPT geometry and components (sectioned to show inner detail.)

B. Motivation and Previous Work

The motivation for developing the AZPPT was to construct a thruster that had the following performance characteristics: $T/P \sim 50$ μN/W, $I_{sp} \sim 500$ s, and $\eta_t \sim 10\%$. Such a thruster would have different mission capabilities than those of conventional (flight-qualified) rectangular-geometry thrusters (compare with the LES 8/9 thruster[8] or the EO-1 PPT (Ref. 9): $T/P \sim 15$ μN/W, $I_{sp} \sim 1000$ s, and $\eta_t \sim 7\%$.)

Our approach to increasing T/P was to increase the amount of propellant surface area exposed to the arc. However, this strategy can drastically decrease the thrust efficiency because increasing propellant surface area could substantially decrease the propellant utilization efficiency. Mass (or propellant) utilization efficiency in ablative PPTs is low (<50%) as a result of two processes—late-time vaporization and macroparticle ejection.[5] It has been shown that macroparticles can account for over 30% of the total mass bit in APPTs.[5] In a rectangular-geometry thruster, macroparticles that leave the surface of the propellant (after the discharge is finished) are free to leave the thruster, thus detracting from the propulsive efficiency. The AZPPT geometry can ameliorate this loss mechanism by reducing the free-flight solid angle presented to the propellant surface. Rather than being lost to space at low speed, macroparticles could potentially be confined (trapped) within the thrust chamber, eventually coming to rest on the propellant surface or electrodes. This redeposited propellant would, ideally, be available for acceleration in subsequent discharges. Although the process of ablating the redeposited propellant from the interior cavity surfaces can be quite different from the ablation process for bulk PTFE, the mass utilization is certainly higher for this case than if the macroparticles had instead escaped. In the present study, it was postulated that if the macroparticle loss mechanism could be reduced using the z-pinch geometry, T/P could be increased without negatively impacting the overall efficiency by increasing the amount of exposed propellant surface area.

The AZPPT is attractive because it is compact and simple, possessing no moving parts. The tight coupling of the capacitor directly to the discharge chamber results in low parasitic inductance and, hence, efficient energy transfer from the capacitor to the discharge.[10] The cylindrical propellant bar used in the AZPPT allows for the construction of a thruster that possesses the greatest volume of propellant for a given "footprint" size on a spacecraft. One price for these attractive features is that the propellant geometry changes in time, causing the performance to vary over a mission lifetime. This variation, however, can be characterized a priori for use in the design of a mission.

Historically, rectangular-geometry PPTs have been the most actively researched ablative PPTs (for example, see Refs. 8, 9, and 11). More recently, Burton and coworkers[12–15] achieved high T/P

using a coaxial geometry thruster with a nozzle, and Mikellides and Turchi[16] constructed an inverse z-pinch thruster to test the predictions of analytical optimization models. Of these two, the AZPPT is more similar to Burton's thrusters, with the following four main differences: 1) Burton et al. attempted to optimize their devices as electrothermal accelerators by using dielectric nozzles to recover the thermal energy of the plasma, whereas no nozzle was ultimately retained in the AZPPT design: 2) the cathode in Burton's devices was mounted far from the propellant discharge chamber at the end of the aforementioned nozzle, while the AZPPT's cathode was in direct contact with the propellant bar; 3) Burton's thrusters used side-fed rectangular bars, whereas the AZPPT employed a fixed cylindrical propellant bar; and 4) the capacitor was connected to the electrodes using coaxial cable in Burton's thrusters, whereas the capacitor was directly attached to the discharge chamber in the AZPPT.

C. Design Details

Tests were conducted using two different low-inductance Maxwell capacitors (33.6 and 38.3 μF). All electrodes were constructed from brass, except the AZPPT4 cathode, which was constructed from aluminum. In preliminary testing an aluminum anode was used, but visual inspection revealed signs of excessive wear and pitting. Brass anodes did not show signs of similar wear and were used throughout the testing. Neither the brass nor the aluminum cathodes showed signs of excessive wear.

Three iterations on the basic AZPPT design illustrated in Fig. 1 (AZPPT2-4) were tested for the purpose of gaining insight into how the discharge chamber height-to-width ratio (aspect ratio) and electrode geometry influenced performance. Two different anode and cathode geometries were tested in AZPPT2. In addition to the flat anode and orifice cathode illustrated in Fig. 1, a spike anode and nozzle cathode were tested (see Fig. 2). The nozzle cathode possessed an exit-to-throat area ratio of approximately 10 to 1 and was constructed to test whether any thermal energy in the AZPPT exhaust could be recovered to produce thrust. We speculated that the spike anode would aid in the conversion of radial plasma compression to axial streaming motion (flow turning). The Republic Aviation Corporation used a similar geometric approach to turn plasma flows in their pinch engine.[17] We further speculated that if the arc moved away from the PTFE surface quickly and became concentrated at the spike anode tip the propellant heating rates would be reduced, thus reducing late-time vaporization.

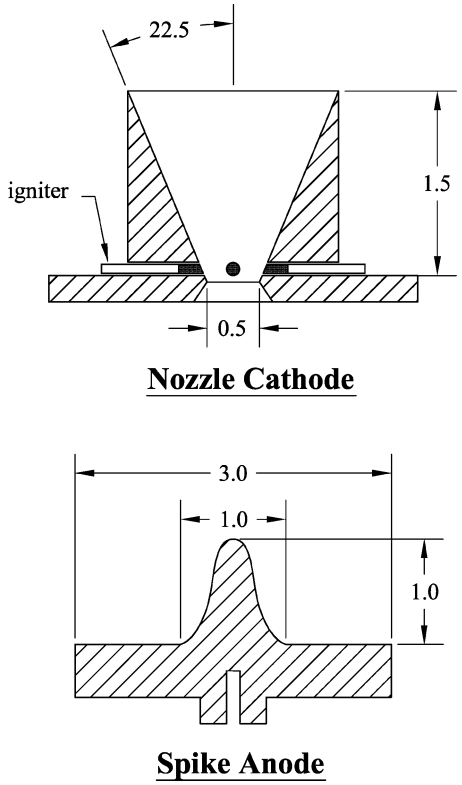

Fig. 2 Schematics (cross sections) of the AZPPT2 nozzle cathode and spike anode (all dimensions in inches).

Table 1 Discharge chamber height, propellant bar outer diameter (o.d.), anode spike height, and cathode orifice diameter

Dimension	AZPPT2	AZPPT3	AZPPT4
Height, in.	1.5	2.25	3.0
o.d., in	3.0	2.5	3.0
Spike, in	1.0	1.5	1.5
Cathode, in	0.5 (nozzle) 0.8 (orifice)	0.9, 2.0	2.5

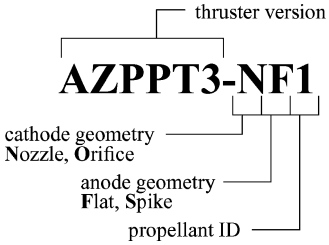

Fig. 3 Shorthand for thruster geometry.

Performance testing of AZPPT2 (see Sec. IV.B) found that only the combination of an orifice cathode and spike anode yielded a value of I_{sp} near the target value. However, corresponding values of T/P and efficiency were both well below their respective target values. AZPPT3-4 retained the AZPPT2 orifice/spike electrode arrangement in an attempt to maintain the specific impulse of AZPPT2, but were constructed with larger discharge chamber aspect ratios to increase T/P and efficiency by exposing more of the propellant surface to the arc. For completeness, the discharge chamber dimensions for AZPPT2-4 are listed in Table 1.

To more easily refer to a specific thruster geometry, the shorthand in Fig. 3 will be used in subsequent sections.

As an example, the label for Fig. 3 refers to the AZPPT3 thruster with a nozzle cathode, flat anode, and 1-in. propellant inner diameter.

III. Experimental Apparatus and Diagnostics

A. Vacuum Facility

A fiberglass vacuum vessel approximately 25 ft in length with a test section diameter of 8 ft was used in this study. The vessel possesses an internal volume of approximately 27,000 liters and uses a diffusion pump with a liquid nitrogen-cooled backstreaming trap to achieve a base pressure of $\sim 5 \times 10^{-6}$ torr. Because of the small mass bits characteristic of PPTs, special care was taken to accurately quantify the level of contaminants (e.g., diffusion pump oil) deposited in the AZPPT thrust chamber between shots. Using a UTI-100 residual gas analyzer, we determined that the mass of contaminants deposited between shots was about five orders of magnitude lower than the propellant mass bit. Therefore, we neglected any error in the mass bit caused by oil deposition on the propellant bar between shots. However, although contamination between consecutive shots is negligible, long-term exposure to atmospheric or untrapped vacuum conditions initially yields biased impulse bit measurements and required the decontamination procedure described in Secs. III.C and IV.B.

B. Thrust Stand

A swinging-gate style microbalance thrust stand capable of measuring extremely small impulse bits was used to measure thruster performance. This stand is the latest design iteration in a series of microthrust stands that include an earlier one at EPPDyL[18] and one designed by EPPDyL for NASA-Jet Propulsion Laboratory.[19] A linear voltage displacement transducer was used to measure and record the position history of the swinging gate. Following Cubbin et al.,[18] the position histories were analyzed to obtain impulse bit measurements. Impulse bits on the order of $\sim$100 μN-s with an error of

10% have been measured using this thrust stand. The uncertainty in the impulse bit measurement was primarily caused by random, or shot-to-shot, variations.

C. Mass Bit Measurement

The average mass bit (change in propellant mass during a test run divided by the number of shots) was used in our performance calculations. Propellant bar masses were measured using a Mettler Instrument Corporation balance having an accuracy of ±30 mg. The pretest measurement was performed after exposing the bar to vacuum for roughly two hours and firing several shots to desorb any trapped gases, and both the pretest and posttest measurements were performed as soon as the vacuum tank was vented to prevent gases from reabsorbing.

The error on the mass bit measurement is primarily systematic in nature. As the thruster is pulsed, the propellant bar experiences a transient period where the temperature and mass bit both increase.[20] Because our experiments were all of short duration (~2000 shots), it was possible that the average mass bit did not represent the true steady-state value. However, the average mass bit from a 4000-shot trial at a pulse energy of 25 J matched the corresponding 2000-shot mass bit within the error bar. Based on this agreement, we concluded that transient propellant temperature effects did not contribute to the error on the mass bit. (Note that the performance changes as ablation increases the discharge chamber diameter. This implies that extremely long-duration trials might not yield accurate steady-state mass bit values and might, in fact, introduce additional uncertainty into that measurement.)

Electrode erosion can also introduce error into the mass bit measurement. However, a measure of the erosion rate has not been made because 1) the changes in electrode mass caused by electrode erosion and PTFE redeposition cannot be distinguished from one another in the limited number of shots performed and 2) we found no suitable method for removing the charred PTFE from the electrodes without also removing electrode material. A measurement of the erosion rate would require the firing of many more shots (100–1000 times as many as were performed in this study) to allow for a distinction between electrode erosion and PTFE redeposition. This measurement is beyond the scope of the present performance study, but an upper bound on erosion's contribution to the mass bit error can be estimated based on published PPT erosion rate data. Assuming that AZPPT erosion occurred in a spot-attachment mode with an average mass loss of 10 μg/C (from Ref. 21) and taking the arc to operate at 60 kA for 10 μs (a conservative estimate), we calculate that the erosion rate has an upper bound of 12 μg/shot (total for two electrodes). We therefore expect electrode erosion to introduce an additional ±7% error, at most, into the smallest mass bit measurements.

D. Current Monitoring

An air core Rogowski coil (for example, see Ref. 22) was constructed to monitor the AZPPT discharge current. The 80-turn coil, possessing an inductance of 1.2 μH and a series resistance of 0.27 Ω, was integrated into the AZPPT structure as illustrated in Fig. 1. Integration of the raw probe output was performed numerically to yield a current waveform. The coil was calibrated against the output of a Pearson 4100 current monitor. The value of the calibration constant, which multiplies the integrated Rogowski coil waveform, was $2.06\ (\pm 0.15) \times 10^8$ A/V^{-1}s^{-1}.

E. High-Speed Photography

To better understand the current sheet dynamics, a modified version of AZPPT2-OS1 was constructed using a copper-mesh sidewall and clear acrylic propellant to allow optical access into the discharge inside the thruster. Imaging of the discharge in this thruster was performed using a Hadland Photonics Imacon 792/LC camera set to a framing rate of 500 kHz and an exposure time per frame of 400 ns. By adjusting the camera timing, photographs were obtained showing how the luminous portion of the discharge evolved spatially during the entire pulse.

IV. Experimental Results

A. PTFE Surface Observations

Before discussing the quantitative measurements, we briefly describe the general appearance of the PTFE bar. Sooting was observed on the bar, but it was localized near the anode with a cleaner surface exposed near the cathode. (Note that charred PTFE never shorted the electrodes in the thousands of shots fired.) The azimuthal ablation appeared symmetric, implying that the thruster was not preferentially breaking down near one igniter, and the photographs of the discharge do not indicate any spoking. Axially, ablation near the cathode appeared to be greater.

Quantitative evaluation of the evolution of the ablation profile would require hundreds of thousands of shots and is beyond the scope of this study. Numerical simulations, however, give some insight into a mechanism that could create the ablation profile just described. Modeling of this thruster (see Sec. V) and other electrothermal APPTs with similar discharge characteristics[23,24] indicates that approximately 90% of the heating of the PTFE face is caused by particle convection while the remaining 10% is caused by radiation. The source of "hot" particles and plasma radiation is the pinched region between the anode tip and the cathode, where Joule heating is greatest. The PTFE wall is most heated and consequently would ablate at a greater rate in the region near the cathode because of its close proximity to the hot, pinched region.

B. Thruster Performance

The impulse bit was measured at selected intervals between which the thruster was pulsed at a frequency of 0.5 Hz. The impulse bit was observed to asymptote to a constant value after about 10 shots. (The first several shots yielded impulse bits approximately 25% higher than the steady-state value, most likely because of surface contamination.[19,25] To avoid a biasing of the results as a result of contamination, data points before shot 100 were excluded from the analysis. The impulse bit was taken as the average of about 50 data points acquired intermittently between shot numbers 100 and 2000, although the asymptotic value of the impulse bit was verified up to shot number 4000 in some cases.

Table 2 lists the AZPPT configurations tested, and Fig. 4 presents a complete summary of the performance of AZPPT2-4. Specific impulse I_{sp}, thrust-to-power (T/P), and thrust efficiency η_t were

Table 2 Test configurations corresponding to the data presented in Fig. 4

Configuration no.	Geometry	C, μF	E, J
1	AZPPT2-OF1	38.3	76
2	AZPPT2-OF1.5	38.3	76
3	AZPPT2-NF1	38.3	76
4	AZPPT2-NF1.5	38.3	76
5	AZPPT2-OS1	38.3	76
6	AZPPT2-OS1.5	38.3	76
7	AZPPT2-NS1	38.3	76
8	AZPPT3-OS1	33.6	25
9	AZPPT3-OS1	33.6	50
10	AZPPT3-OS1	33.6	67
11	AZPPT3-OS1.5	33.6	25
12	AZPPT3-OS1.5	33.6	50
13	AZPPT3-OS1.5	33.6	67
14	AZPPT3-OS1	38.3	25
15	AZPPT3-OS1	38.3	50
16	AZPPT3-OS1	38.3	67
17	AZPPT3-OS1	38.3	76
18	AZPPT3-OS1.5	38.3	25
19	AZPPT3-OS1.5	38.3	50
20	AZPPT3-OS1.5	38.3	67
21	AZPPT3-OS1.5	38.3	76
22	AZPPT4-OS1	33.6	25
23	AZPPT4-OS1	33.6	50
24	AZPPT4-OS1	33.6	67
25	AZPPT4-OS1.5	33.6	25
26	AZPPT4-OS1.5	33.6	50
27	AZPPT4-OS1.5	33.6	67

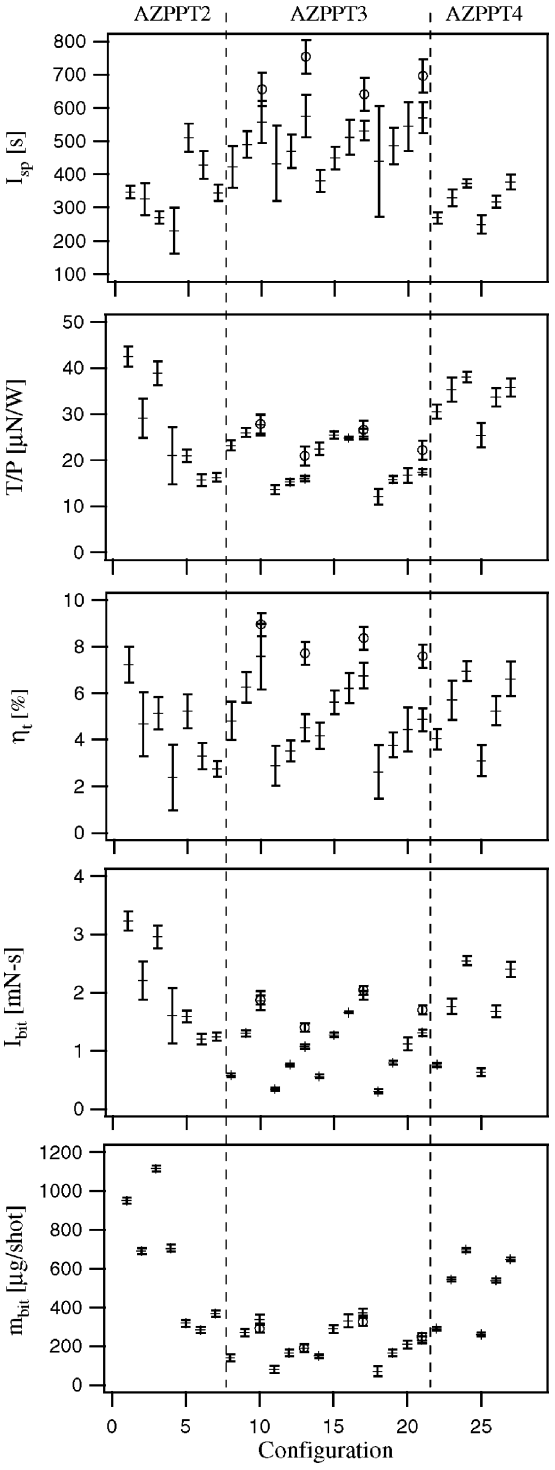

Fig. 4 Summary of performance data. (Note that the specific impulse and mass bit errors do not include electrode erosion.)

all evaluated according to their standard definitions.[10] The error bars in Fig. 4 were evaluated according to the ISO standard[26] and represent a 95% confidence interval. (Note that the specific impulse and mass bit errors do not include electrode erosion.)

The most drastic geometric variations were tested in AZPPT2. Recalling the performance goals defined earlier, Fig. 4 shows that only AZPPT2-OS1 met any of the specified design goals ($I_{sp} \sim 500$ s); however, T/P and η_t for this configuration were far below the target values.

It was surprising that the performance of AZPPT2 with the nozzle cathode was lower than with a simple orifice. However, as will be discussed next, the performance of the AZPPT was later found to decrease as the cathode orifice diameter was decreased. So, the nozzle's slightly smaller orifice (throat diameter = 0.5 in.) might have lowered its performance relative to the thruster with a simple orifice (diameter = 0.8 in.) Because increasing the throat diameter would have reduced the effectiveness of the nozzle by decreasing the area ratio, the nozzle cathode was not implemented in later AZPPT iterations. Also note that the mass bits for all of the flat anode cases are much larger than those for the spike anode cases. Although this is not conclusive evidence, it certainly supports our notion (see Sec. II.C) that the spike anode could help reduce late-time propellant inefficiencies.

In AZPPT3, the orifice-cathode/spike-anode combination was retained, but the discharge chamber aspect ratio (ratio of height to diameter) was increased relative to that of AZPPT2. Also, we tested two cathode orifice diameters (the data for the larger diameter are indicated by the circular data points on Fig. 4 in configurations 10, 13, 17, and 21), two different capacitors, and four different initial capacitor energies. We found that 1) all performance parameters were maximized for the larger cathode orifice and highest energy, 2) there was a slight overall increase in performance when the lower valued capacitor was employed, and 3) there was a slight decrease in T/P and η_t at the larger propellant diameter. AZPPT3 exceeded the performance of AZPPT2 in all categories (compare configs. 5 and 6 with 17 and 21). The peak I_{sp}($\sim$ 650–750 s) exceeded the design goal, and the peak η_t($\sim$ 8–9%) approached the design goal. However, the T/P showed only about a 25% increase over AZPPT2—about half of the desired value.

In AZPPT4, the discharge chamber aspect ratio was increased relative to AZPPT3. Also, the diameter of the cathode was increased, and the cathode orifice was maximized so that most of the top surface of the propellant was exposed to the arc. The 33.6-μF capacitor was employed based on its performance edge in the AZPPT3 thruster. The data in Fig. 4 indicate that the modifications implemented in AZPPT4 increased the thrust-to-power ratio by over 30%, to a maximum value of 37 μN/W. However the corresponding values of I_{sp} and η_t dropped to under 400 s and 7%, respectively, at the highest pulse energy. As before, all performance parameters increased with discharge energy. Also, the values of T/P and η_t decreased slightly at larger propellant diameters.

We would like to mention that we also tested a second propellant: glass-filled PTFE (25% glass). We speculated that the higher melting temperature of glass might further mitigate some of the late-time vaporization issues and yield better performance. Unfortunately, our limited testing showed that the impulse bit did not rapidly reach a steady-state value, as in the case of pure PTFE, indicating that the propellant surface conditions were continuing to evolve over the duration of a few thousand shots. The trends in the data did, however, point toward higher specific impulse. Further studies with this propellant are recommended.

C. Discharge Current

Current waveforms typical of those measured in AZPPT2-4 are given in Fig. 5, and the circuit parameters of each successive thruster

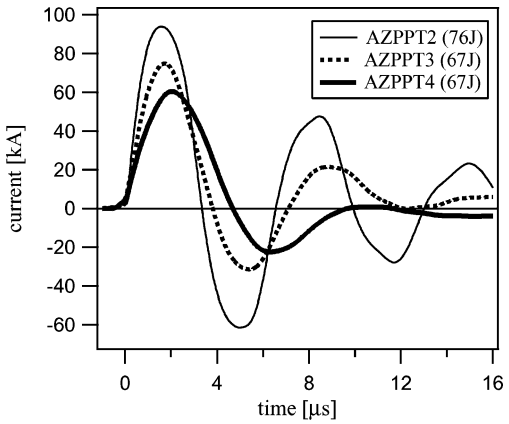

Fig. 5 AZPPT discharge current waveforms.

Table 3 Circuit parameters and ringing frequencies computed from curve fits of the current waveforms given in Fig. 5

Case	C, μF	L, nH	R, mΩ	f, kHz
AZPPT2 (76 J)	38.3	29	7	151
AZPPT3 (67 J)	33.6	37	18	142
AZPPT4 (67 J)	33.6	57	25	115

generation are summarized in Table 3. The waveforms exhibit the damped sinusoidal behavior typical of ablative PPTs. Notice that the peak current and ringing frequency decreased in each successive iteration of the AZPPT indicating increased inductance. The damping coefficient also increased in each generation of the thruster because of increased energy dissipation. Greater dissipation implies a better impedance match between the capacitor and the thruster or, more generally, a higher electrical efficiency. Increased dissipation also serves to reduce current oscillations, which can be problematic for reasons other than poor electrical efficiency—current reversals tend to lower the lifetime of capacitors. Additionally, a current reversal, and its associated high dI/dt, can cause the arc to restrike at the point of lowest inductance, namely, the propellant face, causing further propellant ablation and lowering the mass utilization efficiency. Finally, the restrike current could interact with the original pinched current flowing at the thruster center to form a current loop inside the discharge chamber. The magnetic field trapped within this loop would impart an outward force on the restrike current pushing it into the propellant face and potentially causing enhanced, but undesirable, ablation of the PTFE.

D. High-Speed Photography

The modified version of AZPPT-OS1 was positioned in the vacuum tank so that a side view of the discharge could be photographed. A 590-nm interference filter (which corresponds to a strong carbon ion line[27]) was placed over the camera lens in order to image only ion emission and, presumably, more accurately define the location of the current sheet. Figure 6 shows a sequence of photographs obtained during a single discharge event. The indicated times can be compared with the current waveform in Fig. 5 to determine the corresponding current level. The images show that the discharge initially extended the length of the chamber, while later in time the current remained focused at the tip of the spike. The luminosity from the plasma is not necessarily indicative of the current path. However, a recent study by Markusic et al.,[28] in which magnetic fields were directly measured in an electromagnetic accelerator and then compared to a photographic survey of the discharge, did find that the luminous region of the plasma in their experiment correlated to the actual current path. It is, therefore, possible that a similar correlation exists in the AZPPT.

V. Numerical Modeling

A. AZPPT Model

A numerical model was constructed to gain insight into the operation of the AZPPT. Modeling of the PTFE chamber included plasma generation processes (ablation, heating, radiation, ionization, etc.) and plasma acceleration. The main features of the plasma flow were determined by kinetic and hydrodynamic phenomena such as Joule heating, heat transfer to the dielectric, PTFE ablation, and electrothermal acceleration of the plasma up to the sound speed at the cavity exit. The current distribution in the pinched region was varied parametrically to obtain a current density for use in an energy balance. A schematic representation of the geometry modeled is given in Fig. 7.

The time constant for pinching can be estimated as[29]

$$\tau = (\mu\rho)^{\frac{1}{4}} \left(\frac{\Delta}{dI/dt} \right)^{\frac{1}{2}} \tag{1}$$

where dI/dt is the current rise rate. For typical AZPPT discharge parameters the current is strongly pinched for times greater than

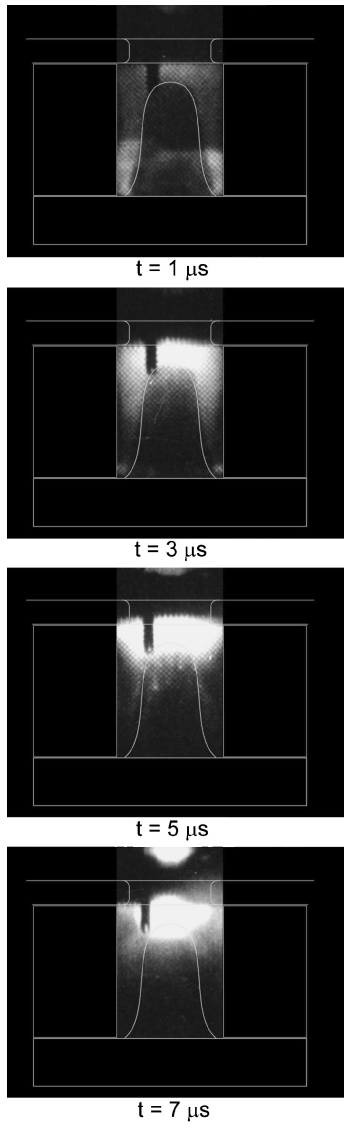

Fig. 6 Sequence of high-speed photographs of the discharge inside AZPPT2 with transparent Plexiglas® propellant and mesh sidewalls. (Thruster sketched for clarity. Dark object protruding down into the plasma is a structural member inside the Plexiglas®). Photos obtained using a 590-nm filter.

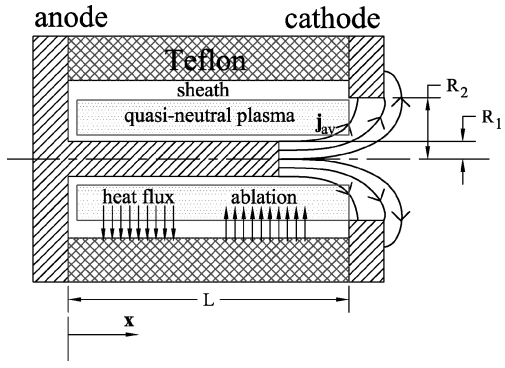

Fig. 7 Schematic of the simplified AZPPT geometry adopted for the model.

100 ns (note that the photographic data presented in Fig. 6 supports this conclusion). Because the pinching time was much shorter than the length of the discharge ($\sim$15 μs), we assumed that the current was always fully pinched.

PTFE ablation is modeled following Ref. 30. The mathematical description included models of two different layers between the surface and the plasma bulk: 1) a kinetic nonequilibrium layer conforming to the surface with a thickness of about one mean free path and 2) a collisionally dominated layer in thermal and ionization nonequilibrium. An electrical sheath model is also included in the

plasma-wall transition layer. The ablation rate is given as[30]

$$\Gamma = mV_1 n_1 = n_1 \left(\frac{k}{m} \frac{n_2 T_2 - n_1 T_1}{n_1 - n_1^2/n_2} \right)^{\frac{1}{2}} \quad (2)$$

where m is an effective mass of an atom in atomic mass units (an average between 12 for C and 17 for F). The values of n_2 and T_2 were determined by the plasma bulk flow and an energy balance (see below), while n_1 and T_1 were found through the solution of the kinetic layer problem.[31] The system of equations is closed if the equilibrium vapor pressure is specified, thus fixing the conditions at the PTFE surface.

A general plasma flow model was previously presented.[23,32] This model was simplified by assuming that all parameters in the AZPPT varied in the axial direction z, but were uniform in the radial direction. Additionally, the spike anode was modeled as a right circular cylinder of radius R_1. The axial mass and momentum conservation equations are

$$A\left(\frac{\partial \rho}{\partial t} + \frac{\partial (\rho V)}{\partial z} \right) = 2\pi R_2 \Gamma(t, z) \quad (3a)$$

$$\rho\left(\frac{\partial V}{\partial t} + V \frac{\partial V}{\partial z} \right) = -\frac{\partial P}{\partial z} \quad (3b)$$

where A is the cross-sectional area of the PTFE chamber ($A = \pi[R_2^2 - R_1^2]$), and $\Gamma(t, z)$ is the instantaneous local ablation rate.

Energy transfer from the plasma column to the PTFE cavity wall consisted of particle fluxes and radiative heat transfer. An energy balance can be written in the form[23]

$$\frac{3}{2} n_e \left(\frac{\partial T_e}{\partial t} + V \frac{\partial T_e}{\partial z} \right) = Q_J - Q_r - Q_F \quad (4)$$

We assumed that Joule heating, which is controlled by current density, was concentrated in the pinched region near the anode tip. Following Ref. 33, plasma radiation was modeled as a continuous spectrum. We set $\partial T_e/\partial z$ equal to zero because a previous publication[34] and our own estimates showed that electron temperature varied only slightly with axial position. The temperature fields inside the PTFE wall and at the PTFE surface were calculated following Refs. 23 and 32.

The chemical plasma composition was found by assuming local thermodynamic equilibrium and following Refs. 23, 35, and 36. Because PTFE molecules C_2F_4 dissociate at the electron temperatures (1-4 eV) and plasma densities (10^{22}–10^{24} m^{-3}) we expected to obtain in the AZPPT, our initial gas composition consisted of only C and F atoms. The Saha equations for each species (C and F) were supplemented by conservation of nuclei and quasi-neutrality constraints.

The total current $I(t)$ was modeled based upon the waveform measured in AZPPT3 (see Fig. 5). In general, the two-dimensional current density distribution in the pinched region between the anode tip, where the current density is $j_a = I/\pi R_1^2$, and the cathode could be calculated using the magnetic transport equation. However, in the present one-dimensional model of the plasma flow only the average current density was considered. The variable α, which was defined as the ratio between the average current density in the pinched region and the current density at the anode spike tip (j_{av}/j_a), was varied parametrically to obtain solutions to the numerical model. Physically, α also represents the ratio of the pinching force ($\boldsymbol{j} \times \boldsymbol{B}$) to the plasma pressure. In our simulations, α was varied between 0.2 to 1.2. Cases for which $\alpha > 1$ are physically reasonable because only the plasma pressure limits current constriction.

The simulations were performed assuming a freestream condition at the thruster exit (i.e., the plasma velocity equaled the local sound speed at $x = L$). Thruster performance characteristics such as mass bit, impulse bit, and average specific impulse were obtained by integrating the computed plasma parameters over the 15-μs pulse.

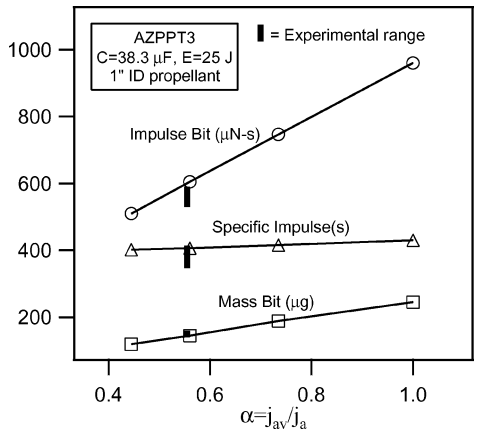

Fig. 8 AZPPT3 performance as a function of average current density to the anode current density ratio and comparison with experiment (○, △, □, correspond to simulated cases).

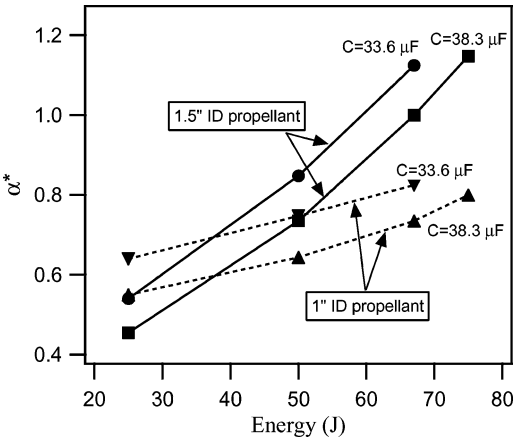

Fig. 9 Average current density to the anode current density ratio (α^*) for which the model agrees with experiment as a function of the pulse energy with capacitance and propellant i.d. as parameters.

B. Calculated Performance

Performance characteristics obtained from simulations of AZPPT3 operating at 25 J are shown in Fig. 8. The impulse bit and mass bit strongly increase as a function of α. The measured performance shows good agreement with the simulations for $\alpha \approx 0.55$. This result suggests that the average current density in the pinched area is much lower than j_a.

Simulations were performed for the entire experimental range of AZPPT3 pulse energies and propellant diameters. The results are summarized in Fig. 9, where α^* is the value of α for which agreement with the measured impulse bit was obtained. Generally the average current density needed for agreement increases with pulse energy. This occurs because the current, and hence the pinching force ($\boldsymbol{j} \times \boldsymbol{B}$), increases with increasing energy. Also, as the pulse energy is increased the value of α^* grows significantly faster for the larger PTFE chamber i.d. This happens because the ablation rate, and consequently the plasma density and pressure, in the larger propellant diameter case grows more slowly as energy is increased.

The dependence of T/P on the PTFE chamber length l was calculated holding the pinch region length constant as the chamber and anode spike lengths were varied (see Fig. 7). The results of these calculations are given in Fig. 10. The T/P for the smaller propellant i.d. is much higher than that for the larger propellant i.d. Also, the variation of T/P with pulse energy is relatively moderate for the 1-in. i.d. propellant while T/P significantly increases with pulse energy for the 1.5-in. i.d. propellant. For each diameter,

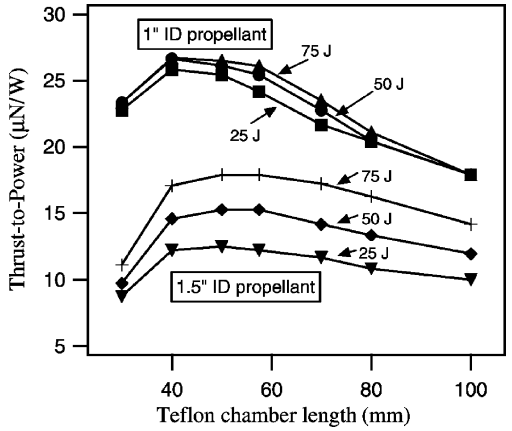

Fig. 10 Thrust-to-power ratio (T/P) as a function of the PTFE chamber length with pulse energy and the propellant i.d. as parameters. $C = 38.3\ \mu$F.

there exists a PTFE chamber length corresponding to a maximum T/P ($l \sim 40$ mm for the 1-in. i.d. case and $l \sim 50$ mm for the 1.5-in. i.d. case). As l is increased further, T/P decreases, dropping quite rapidly for the smaller propellant i.d. The decrease of T/P with increasing chamber length is mainly caused by lower plasma heating in the channel because the length of the pinched area normalized by the total length of the propellant decreases as l is increased. These results cannot easily be correlated with the experimental data presented earlier because, as shown in Table 1, the length of the pinch area was not constant in AZPPT2-4.

C. Summary of Numerical Results

A simplified one-dimensional model of an AZPPT in which the average current density in the pinched area was varied parametrically can reasonably predict the plasma parameter evolution and performance. The model predicts that the electron temperature peaks at about 4 eV and the plasma density peaks at about 8×10^{23} m^{-3}. During the initial stage of the discharge, the plasma is strongly ionized, whereas in late time the ionization fraction peaks at about 0.5. Our results suggest that the current in the pinched area is more constricted in the case of higher pulse energies. In addition, current constriction increases with increasing propellant inner diameter. Thrust-to-power ratio is higher in the case of smaller propellant i.d., which is in agreement with the experimental data. The model predicts a PTFE chamber length that maximizes the thrust-to-power ratio. The nonmonotonic behavior of T/P as a function of chamber length is more pronounced in the case of a smaller propellant inner diameter.

VI. Conclusions

We developed and tested a series of ablative z-pinch PPTs for the purpose of creating a thruster with higher thrust-to-power ratios than more common PPT designs. Three design iterations resulted in thrust-to-power ratios ranging from 12–45 μN/W, with specific impulse and thrust efficiency spanning 240–760 s and 2–9%, respectively. Numerical modeling showed reasonable quantitative agreement with the experimental data and pointed to a primarily electrothermal acceleration mechanism.

The following conclusions were reached in this study:

1) Flow turning was realized in the ablative z-pinch thruster geometry, yielding an axial flow that produced useful thrust.

2) The AZPPT's overall performance was maximized through the use of an orifice cathode and spike anode.

3) Photographic and numerical evidence suggested that the current channel remained constricted near the anode spike tip during most of the discharge.

4) Increasing the aspect ratio of the discharge chamber led to a higher thrust-to-power ratio.

5) Performance was maximized for a larger cathode orifice.

6) The scaling of I_{sp}, T/P, and η_t was such that all increase monotonically with increasing initial capacitor energy.

7) Numerical modeling predicted the existence of an optimal thrust chamber aspect ratio that maximizes the thrust-to-power ratio—providing direction for the construction of future AZPPTs.

VII. Recommendations for Future Work

For all tests, the measured AZPPT performance never met or exceeded more than one of the design goals. In light of this point, the following question can be posed: can further geometric alterations yield a thruster with the desired performance? We do not believe so. Extrapolating from the data, we believe the AZPPT4 geometry operating at 75 J could be refined to produce, at best, a thruster with $I_{sp} \sim 500$ s, $T/P \sim 33\ \mu$N/W, and $\eta_t \sim 8\%$. However, item 6 in the preceding conclusions indicates a path to a thruster that satisfies all of the design goals—increased pulse energy. For example, extrapolating (linearly) the AZPPT4 performance trends in Fig. 4 suggests that AZPPT4 pulsed at an initial energy of approximately 130 J would have $T/P \sim 50\ \mu$N/W, $I_{sp} \sim 525$ s, and $\eta_t \sim 12\%$. We therefore recommend that future studies of the AZPPT explore high pulse energies.

Acknowledgments

We gratefully acknowledge Aerojet (Redmond, Washington) for supplying the capacitors used during these experiments and Chris Waters of Pearson Electronics (Palo Alto, California) for many helpful discussions regarding current measurement techniques. We also acknowledge Robert Sorenson, Christine McLeavey, and Joshua Levine for their contributions to this work.

References

[1]Burton, R. L., and Turchi, P. J., "Pulsed Plasma Thruster," *Journal of Propulsion and Power*, Vol. 14, No. 5, 1998, pp. 716–735.

[2]Martinez-Sanchez, M., and Pollard, J. E., "Spacecraft Electric Propulsion—An Overview," *Journal of Propulsion and Power*, Vol. 14, No. 5, 1998, pp. 688–699.

[3]Polzin, K. A., Choueiri, E. Y., Gurfil, P., and Kasdin, N. J., "Plasma Propulsion Options for Multiple Terrestrial Planet Finder Architectures," *Journal of Spacecraft and Rockets*, Vol. 39, No. 3, 2002, pp. 347–356.

[4]Morring, F., Jr., "EO-1 Satellite Demonstrates Autonomous Formation Flying," *Aviation Week and Space Technology*, Vol. 154, No. 21, 2001, pp. 46, 48, 49.

[5]Spanjers, G. G., Lotspeich, J. S., McFall, K. A., and Spores, R. A., "Propellant Losses Because of Particulate Emission in a Pulsed Plasma Thruster," *Journal of Propulsion and Power*, Vol. 14, No. 4, 1998, pp. 554–559.

[6]Liebermann, M. A., De Groot, J. S., Toor, A., and Spielman, R. B., *Physics of High-Density Z-Pinch Plasmas*, Springer-Verlag, New York, 1999.

[7]Jahn, R. G., von Jaskowsky, W., and Burton, R. L., "Ejection of a Pinched Plasma from an Axial Orifice," *AIAA Journal*, Vol. 3, No. 10, 1965, pp. 1862–1866.

[8]Vondra, R. J., Thomassen, K. I., and Solbes, A., "Analysis of Solid Teflon Pulsed Plasma Thruster," *Journal of Spacecraft and Rockets*, Vol. 7, No. 12, 1970, pp. 1402–1406.

[9]Benson, S. W., Arrington, L. A., Hoskins, W. A., and Meckel, N. J., "Development of a PPT for the EO-1 Spacecraft," AIAA Paper 99-2276, June 1999.

[10]Jahn, R. G., *Physics of Electric Propulsion*, McGraw–Hill, New York, 1968, pp. 4, 265, 290.

[11]Ebert, W. L., Kowal, S. J., and Sloan, R. F., "Operational Nova Spacecraft Teflon Pulsed Plasma Thruster System," AIAA Paper 89-2497, July 1989.

[12]Bushman, S. S., and Burton, R. L., "Heating and Plasma Properties in a Coaxial Gasdynamic Pulsed Plasma Thruster," *Journal of Propulsion and Power*, Vol. 17, No. 5, 2001, pp. 959–966.

[13]Bushman, S. S., Burton, R. L., and Antonsen, E., "Arc Measurement and Performance Characteristics of a Coaxial Pulsed Plasma Thruster," AIAA Paper 98-3660, July 1998.

[14]Antonsen, E., Burton, R. L., and Rysanek, F., "Energy Measurements in a Coaxial Electromagnetic Pulsed Plasma Thruster," AIAA Paper 99-2292, June 1999.

[15]Rysanek, F., and Burton, R. L., "Effects of Geometry and Energy on a Coaxial Teflon Pulsed Plasma Thruster," AIAA Paper 2000-3429, June 1999.

[16]Mikellides, I. G., and Turchi, P. J., "Optimization of Pulsed Plasma Thrusters in Rectangular and Coaxial Geometries," *International Electric Propulsion Conference*, Electric Rocket Propulsion Society, Fairview Park, OH, 1999, pp. 1232–1239.

[17]Aronowitz, L., and Duclos, D. P., "Characteristics of the Pinch Discharge in a Pulsed Plasma Accelerator," *Electric Propulsion Development*, edited by E. Stuhlinger, Vol. 9, Progress in Aeronautics and Astronautics, Academic Press, New York, 1963, pp. 513–530.

[18]Cubbin, E. A., Ziemer, J. K., Choueiri, E. Y., and Jahn, R. G., "Pulsed Thrust Measurements Using Laser Interferometry," *Review of Scientific Instruments*, Vol. 68, No. 6, 1997, pp. 2339–2346.

[19]Ziemer, J. K., Choueiri, E. Y., and Birx, D., "Is the Gas-Fed PPT an Electromagnetic Acelerator? An Investigation Using Measured Performance," AIAA Paper 99-2289, June 1999.

[20]Spanjers, G. G., Malak, J. B., Leiweke, R. J., and Spores, R. A., "Effect of Propellant Temperature on Efficiency in the Pulsed Plasma Thruster," *Journal of Propulsion and Power*, Vol. 14, No. 4, 1998, pp. 545–553.

[21]Aleksandrov, V. V., Belan, N. V., Koslov, N. P., Mashtylev, N.A., Popov, G. A., and Khvesiyk, V. I., *Pulsed Plasma Accelerators*, Kharkov Aviation Inst., Kharkov, Ukraine, 1983, pp. 82 (in Russian).

[22]Wright, E. S., "The Design and Development of Rogowski Coil Probes for Measurement of Current Density Distribution in a Plasma Pinch.," Dept. of Aerospace and Mechanical Sciences, Princeton Univ., Rept. 740, NJ, June 1965; also M.S. Thesis, May 1965.

[23]Keidar, M., Boyd, I. D., and Beilis, I. I., "Electrical Discharge in the Teflon Cavity of a Coaxial Pulsed Plasma Thruster," *IEEE Transactions in Plasma Science*, Vol. 28, No. 2, 2000, pp. 376–385.

[24]Keidar, M., Boyd, I. D., and Beilis, I. I., "Model of an Electrothermal Pulsed Plasma Thruster," *Journal of Propulsion and Power*, Vol. 19, No. 3, 3002, pp. 424–430.

[25]Ziemer, J. K., "Scaling Laws in Gas-Fed Pulsed Plasma Thrusters," Ph.D. Dissertation, Dept. of Mechanical and Aerospace Engineering, Princeton Univ., NJ, June 2001.

[26]*Guide to the Expression of Uncertainty in Measurement*, International Organization for Standardization, Geneva, Switzerland, 1995.

[27]Markusic, T. E., and Spores, R. A., "Spectroscopic Emission Measurements of a Pulsed Plasma Thruster," AIAA Paper 97-2924, July 1997.

[28]Markusic, T. E., Choueiri, E. Y., and Berkery, J. W., "Measurements of Current Sheet Canting in a Pulsed Electromagnetic Accelerator," *Physics of Plasmas* (accepted for publication, 2004).

[29]Krall, N. A., and Trivelpiece, A. W., *Principles of Plasma Physics*, McGraw–Hill, New York, 1973, p. 126.

[30]Keidar, M., Boyd, I. D., and Beilis, I. I., "On the Model of Teflon Ablation in an Ablation-Controlled Discharge," *Journal of Physics D: Applied Physics*, Vol. 34, No. 11, June 2001, pp. 1675–1677.

[31]Keidar, M., Fan, J., Boyd, I. D., and Beilis, I. I., "Vaporization of Heated Materials into Discharge Plasmas," *Journal of Applied Physics*, Vol. 89, No. 6, 2001, pp. 3095–3099.

[32]Keidar, M., and Boyd, I. D., "Device and Plume Model of an Electrothermal Pulsed Plasma Thruster," AIAA Paper 2000-3430, July 2000.

[33]Kozlov, G. I., Kuznetsov, V. A., and Masyukov, V. A., "Radiative Losses by Argon Plasma and the Emissive Model of a Continuous Optical Discharge," *Soviet Physics: Journal of Experimental and Theoretical Physics*, Vol. 39, No. 3, 1974, pp. 463–468.

[34]Kovatya, P., and Lowke, J. J., "Theoretical Prediction of Ablation Stabilised Arcs Confined in Cylindrical Tubes," *Journal of Physics D: Applied Physics*, Vol. 17, No. 6, 1984, pp. 1197–1212.

[35]Kovatya, P., "Thermodynamic and Transport Properties of Ablated Vapors of PTFE, Alumina, Perspex and PVC in the Temperature Range 5000-30000 K," *IEEE Transactions in Plasma Science*, Vol. 12, No. 1, 1984, pp. 38–42.

[36]Schmahl, C. S., and Turchi, P. J., "Development of Equation-of-State and Transport Properties for Molecular Plasmas in Pulsed Plasma Thrusters. Part I: A Two-Temperature Equation of State for Teflon," *International Electric Propulsion Conference*, Electric Rocket Propulsion Society, Fairview Park, OH, 1997, pp. 781–788.